Chirped Bloch-harmonic oscillations in a parametrically forced optical lattice

Usman Ali,[1] Martin Holthaus,[2] and Torsten Meier[1]
[1]*Department of Physics, Paderborn University, Warburger Strasse 100, D-33098 Paderborn, Germany*
[2]*Institut für Physik, Carl von Ossietzky Universität, D-26111 Oldenburg, Germany*

(Received 16 June 2023; accepted 17 October 2023; published 15 November 2023)

The acceleration theorem for wave packet propagation in periodic potentials disentangles the k-space dynamics and real space dynamics. This is well known and understood for Bloch oscillations and super Bloch oscillations in the presence of position-independent forces. Here, we analyze the dynamics of a model system in which the k-space dynamics and the real space dynamics are inextricably intertwined due to a position-dependent force provided by a parabolic trap. We demonstrate that this coupling gives rise to significantly modified and rich dynamics when the lattice is shaken by a modulated parabolic potential. The dynamics range from chirped Bloch-harmonic oscillations to asymmetric spreading oscillations. We analyze these findings by tracing the spatiotemporal dynamics in real space and by visualizing the relative phase in the k-space dynamics which leads to an accurate explanation of the obtained phenomena. We also compare our numerical results to a local acceleration model and obtain very good agreement for the case of coherent oscillations, however, deviations for oscillations with spreading dynamics which altogether supports the interpretations of our findings.

DOI: 10.1103/PhysRevResearch.5.043152

I. INTRODUCTION

Ultracold atomic gases in optical lattices are ideal model systems for quantum simulations [1]. These systems allow for flexible manipulation of the parameters, interatomic interactions, and lattice defects. Improved measurement techniques have opened doors to new interpretations, effects, and applications of varied phenomena in solid-state physics [1]. Prominent examples that are largely explored in ultracold atomic systems are superfluidity [2], quantum magnetism [3], topological matter [4], Anderson localization [5], and Bloch oscillations [6–8].

In solid-state physics, the acceleration theorem is a fundamental concept that describes the motion of electrons in a crystal under the influence of spatially homogeneous electric fields. The theorem states that for an electronic wave packet that is well localized in k space and is constrained to a single band, the wave packet center $\mathbf{k}_c$ evolves according to $\hbar\dot{\mathbf{k}}_c(t) = -e\mathbf{E}(t)$, where $-e$ is the electronic charge, when an electric field $\mathbf{E}(t)$ is applied [9–12]. The acceleration theorem combined with the Jones-Zener expression of group velocity [13], $v_g(t) = \hbar^{-1} dE/dk|_{k_c(t)}$, devises a powerful method to describe the wave packet motion within a semiclassical framework. Important examples where this method is proven to be highly effective are Bloch oscillations (BOs) [14–21] and super Bloch oscillations (SBOs) [10,22–28]. Considering the dispersion relation of a one-dimensional single-band tight-binding model with hopping amplitude J and lattice period d, $E(k) = -\boldsymbol{J}\cos(kd)$, these dynamics can be summarized by

$$\dot{k_c}(t) = -\frac{1}{\hbar}F(t); \quad \dot{x}(t) = \frac{Jd}{\hbar}\sin(k_c(t)d). \tag{1}$$

For $F(t) = F_0 + F_D\sin(\omega_D t)$ representing the time-dependent force exerted by the electric field, BOs with frequency $\omega_B = F_0 d/\hbar$ are obtained for the case $F_D = 0$ and SBOs appear if $F_D \neq 0$ and the frequency of the oscillating field ω_D is slightly detuned from a rational multiple of ω_B [10].

The key principle behind the separable solutions in these elementary examples is the necessity of a position-independent force. However, in modern experiments with ultracold atoms in optical lattices with parabolic confinement, different situations naturally arise. Thus, position-dependent forces can be realized, which give rise to an intricate interplay between the k-space and real space dynamics. Considering the parabolic confining potential $V(x) = m\omega_\tau^2 x^2/2$, where ω_τ is the trap frequency and m is the atomic mass of the trapped atoms, a local acceleration theorem $\hbar\dot{k}_c(t) = -m\omega_\tau^2 x_c(t)$ can be defined for wave packets located around $x_c(t)$, i.e., slightly away from the center of the parabolic potential, and where the force varies slowly between lattice wells. The resulting dynamics are quite similar to BOs although the evolving wave packet now dephases quite rapidly, which leads to collapse and revivals of BOs [29–36]. These effects are beyond the semiclassical approach; nonetheless, the frequency and amplitude of BOs can be calculated quite generally. The situation becomes even more interesting and complex when the trap potential or the periodic lattice is modulated in time [37,38]. The latter can be utilized to achieve long-range wave packet transport [39], however, a fully consistent analytical theory for the wave packet dynamics in modulated parabolic lattices is not yet available.

In this paper, we analyze the wave packet dynamics in a periodic potential by considering a parametrically modulated parabolic trap. Our analysis shows that the modulation leads to oscillatory transport on top of BOs, for which the predictions of a local acceleration theorem are fairly accurate. These dynamics we denote as chirped Bloch-harmonic oscillations (CBHOs). First, we show dephased CBHOs, where the dephasing follows a different mechanism compared to the dephasing of BOs in static systems. Next, we demonstrate that the dephasing of CBHOs can be suppressed by an initial phase shift in the drive, leading to long-lived coherent CBHOs. Conversely, at the opposite phase of the drive, we observe an asymmetric oscillatory spreading of the wave packet. The spreading motion reveals a new kind of mixed dynamics that exists in the combination of standard BOs and anharmonic BOs. Furthermore, we present an adapted solution to the local acceleration theorem, which highlights the usefulness of the local force assumption in the undriven system and shows good agreement with CBHOs in the driven scenario.

The paper is organized as follows: In Sec. II, we introduce the model and the numerical procedure and provide the parameters used in our calculations. We present, explain, and discuss the obtained results in Sec. III and provide conclusions in Sec. IV.

II. THE MODEL

We consider a condensate of ultracold rubidium atoms in an axially symmetric crossed optical dipole trap, which provides loose axial confinement as compared to tight confinement along the transverse plane. In the limit of strong transverse confinement, and considering the atom-atom interactions are tuned to zero by using the Feshbach resonance, the effective potential in the axial direction is parabolic [40]. In addition, a one dimensional (1D) optical lattice is introduced alongside the parabolic potential, which results in a symmetrically curved periodic potential, see Fig. 1. We assume that the dynamics starts with a rapid displacement of the center of the parabolic potential at time $t = 0$, which together with its subsequent time-dependent modulation can be realized by specialized optical modulators, such as acousto-optic modulator, in the axial beam [41]. Thus, the parabolic potential is modulated periodically, which means that the overall curvature oscillates in time. In dipole and rotating wave approximations, the dynamics of ultracold atomic condensates in the combined potential of a 1D optical lattice and a modulated parabolic trap are effectively described by the Hamiltonian

$$H = \frac{p^2}{2m} + V_0 \sin^2\left(\frac{\pi}{d}x\right) + \frac{1}{2}m\omega_\tau^2 x^2\{1 + \alpha\sin(\omega_D t + \phi)\}, \tag{2}$$

with $t > 0$. Here, V_0 is the depth of the optical lattice and d is the lattice period. Moreover, α, ω_D, and ϕ denote the amplitude, frequency, and initial phase of the driving field, i.e., the oscillatory part of the parabolic potential, respectively.

If the lattice depth is sufficiently high as compared to the atomic recoil energy $E_R = \hbar^2\pi^2/2md^2$, i.e., $V_0 \gtrsim 4E_R$, and the modulation does not induce interband tunneling, one

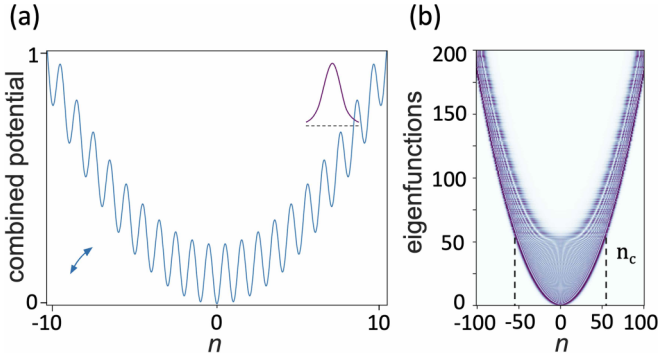

FIG. 1. (a) Schematic diagram showing the combined potential of a 1D optical lattice and an additional parabolic trap. The arrow indicates the oscillating curvature of the combined potential in the presence of a modulation of the trap, and the inset represents a Gaussian wave packet which we consider the starting point of the quantum dynamics. (b) Eigenfunctions of the time-independent system obtained via the stationary solutions of Eq. (3) with the density of each solution placed one over the other as the integer eigennumber is taken on the y axis, and as a function of the real space index n taken on the x axis. The dashed lines at $n = n_c$ mark the separation between harmonic oscillatorlike and strongly localized eigenfunctions.

can express the wave function $\psi(x,t)$ as a superposition of Wannier functions $w(x)$ that are localized in the individual wells at $x = nd$ via $\psi(x,t) = \sum_n c_n(t)\, w_0(x - nd)$. In such a single-band tight-binding description of the system, the dynamics of the complex amplitudes $c_n(t)$ follow from the discrete time-dependent Schrödinger equation and read

$$i\hbar\,\frac{dc_n}{dt} = -\frac{J}{2}(c_{n+1} + c_{n-1}) + K(t)\,n^2 c_n, \tag{3}$$

with $K(t) = K_0(1 + \alpha\sin(\omega_D t + \phi))$, and the parabolicity $K_0 = m\omega_\tau^2 d^2/2$, [29,30]. The symbol J denotes the nearest-neighbor tunneling matrix element, which depends upon the scaled depth of the optical lattice, $s = V_0/E_R$, as $J/E_R \sim 8\,(s)^{\frac{3}{4}}e^{-2\sqrt{s}}/\sqrt{\pi}$ [42,43].

In order to initiate the quantum dynamics, we start with a sudden displacement of the parabolic trap center at time $t = 0$, along the axis of the combined potential. The displacement induces a shift in the mean position of the atomic cloud, and the ensemble starts its journey over the curved periodic wells of the parabolic lattice at $x_0/d = n_0$. For a displacement above the critical index, $n_c = (2J/K_0)^{1/2}$ the energy of the wells is larger than the trap free bandwidth $E > 2J$. In such a regime, the eigenfunctions are increasingly localized in two separate regions of space [44,45], as shown in Fig. 1(b). Without considering a modulation of the trap potential, the expected dynamics would be quite similar to BOs in a locally static force of strength $F_{n_0} \sim -2K_0 n_0/d$ [29,30]. We assume a preparation of the atomic condensate in the regime of strongly localized eigenfunctions away from the center of the parabolic lattice and describe it by a displaced Gaussian wave packet

$$c_n(t=0) = \frac{1}{\sqrt{\sigma_n\sqrt{\pi}}}\, e^{-\frac{(n-n_0)^2}{2\sigma_0^2}}\, e^{-ik_0 n}, \tag{4}$$

with mean position, initial momentum, and spatial width represented by n_0, k_0, and σ_0, respectively. To obtain the

dynamical evolution, we solve Eq. (3) numerically by using the fourth-order Runge-Kutta method for the initial conditions given by Eq. (4). To trace and be able to analyze the wave packet dynamics in k space, we evaluate the Fourier transform

$$c_k(t) = \frac{1}{\sqrt{2\pi}} \int_{-\infty}^{\infty} c_n(t)\, e^{ikn} dn, \tag{5}$$

with k scaled in units of $k_B = 2\pi/d$ and restricted to the first Brillouin zone, i.e., $-1/2 \leqslant k \leqslant 1/2$.

We use values of the system's parameters from an experiment with Bose-condensed ^{87}Rb atoms [46], with atomic mass $m = 1.443 \times 10^{-25}$ kg, which are placed in an optical lattice of period $d = 397.5$ nm with depth $V_0 = 12.77\, E_R$ and a parabolic trap with frequency $\omega_\tau = 2\pi \times 9$ Hz. These values correspond to $J = 0.024\, E_R$, $K_0 = 1.52 \times 10^{-5}\, E_R$, and $n_c \cong 56$. The experimental procedure matches very closely with our assumption of the wave packet preparation, with the only difference that we chose a parabolic optical trap instead of a magnetic trap, and that in our model we consider that the trapping potential can be modulated periodically in time. We start the dynamics from $n_0 = 125$, such that the initial Bloch frequency is given by $\hbar\omega_B = 2K_0 n_0 = 0.0038\, E_R$, which corresponds to $\omega_B = 2\pi \times 13.76$ Hz. A rather wide initial wave packet with a width in real space of $\sigma_0 = 3.16$ corresponding to about 20 appreciably occupied sites and a distance of 7.95μm is considered, which is appropriate for the weak trapping used here. The trap potential is modulated with a strength equal to the static trap strength, i.e., $\alpha = 1$, and the modulation frequency is tuned to exactly match the initial Bloch frequency, i.e., $\omega_D = \omega_B$. As shown below, different dynamics are obtained when tuning the initial phase ϕ of the time-dependent trap potential, which therefore acts as a control parameter.

III. RESULTS AND DISCUSSION

The dynamics obtained for our spatially-inhomogeneous and periodically driven system for $\phi = 0$ is shown in Fig. 2. As seen, the result demonstrates coupled evolution in real and quasimomentum space, where the wave packet's center in one space moves in accordance with the other, and the result corresponds to CBHOs. A slow oscillatory transport combined with standard BOs is observed in Fig. 2(a), which completes its period in 6.5 Bloch periods T_B moving across more than 50 lattice sites in real space. The transport-carrying oscillation highlights the existence of an effective relative phase between the modulation and the BOs in the shaken periodic lattice [28], even though here an external detuning is absent. The dynamics resemble SBOs, however the corresponding evolution in k space, shown in Fig. 2(b), reveals that the relative phase does not sweep around the whole BZ but rather oscillates around its center. The oscillating phase is an outcome of coupling between coordinate position and quasimomentum that manifests itself in the form of parametric modulation of Bloch frequency. In more detail, the relative phase develops from spatial variations, which increase (decrease) the Bloch frequency for wave packet transport against (in) the direction of force. With this, the cycle averaged momentum changes its sign, which flips the transport direction. Accordingly, Bloch frequency starts to decrease (increase) and the phase

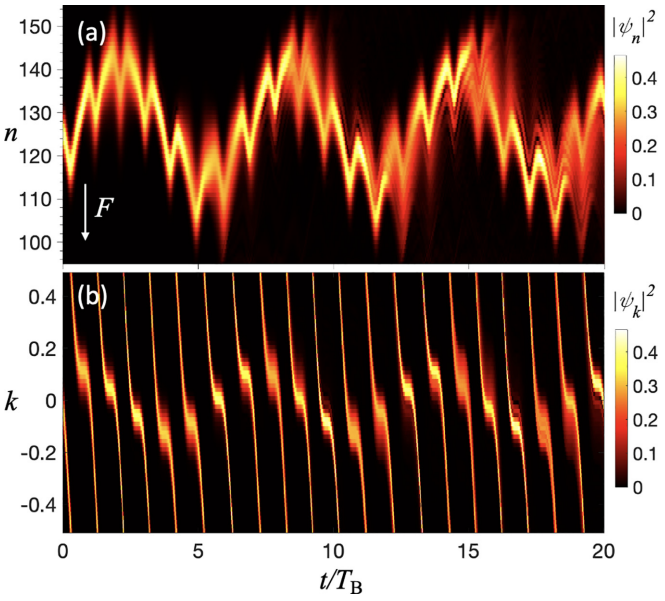

FIG. 2. Time evolution of the absolute square of the wave function in (a) real and (b) quasimomentum space exhibiting CBHOs with some additional weak dephasing. The wave packet starts its journey at $t = 0$ at $n_0 = 125$ with $k_0 = 0$, and we consider a modulated trap potential with drive phase $\phi = 0$.

oscillates. Further, this mechanism repeats itself and cycles continuously. As a result, quick oscillations are generated, and the real space amplitude is low as compared to standard SBOs. Hence, CBHOs can be used to generate oscillatory transport with various amplitudes and temporal periods. Keeping in view the harmonic oscillatorlike profile of oscillatory transport, it is noted that the period of CBHOs, i.e., the chirped Bloch-harmonic period, is independent of the wave packet's initial position and is given by $T_{\mathrm{CBHO}} \sim 2\pi\hbar/\sqrt{JK_0\alpha}$.

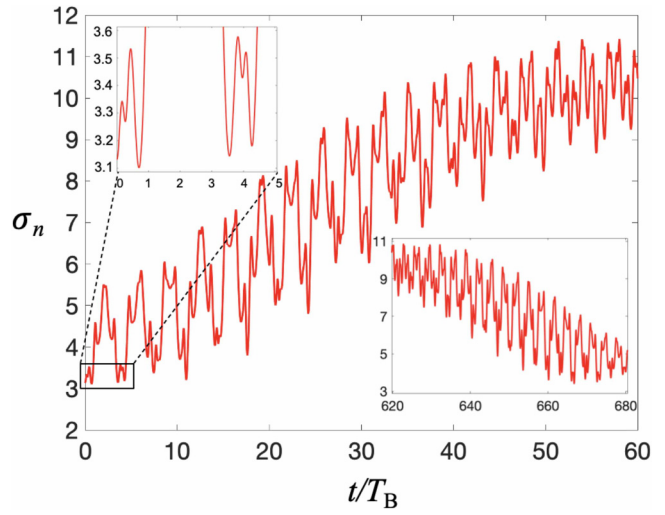

FIG. 3. Width of the wave packet in real space for a drive phase of $\phi = 0$. The left inset shows a magnified image of the width during the first five Bloch periods. The inset on the right displays the long-time evolution of the width, which shows a decline of the width corresponding to a complete revival.

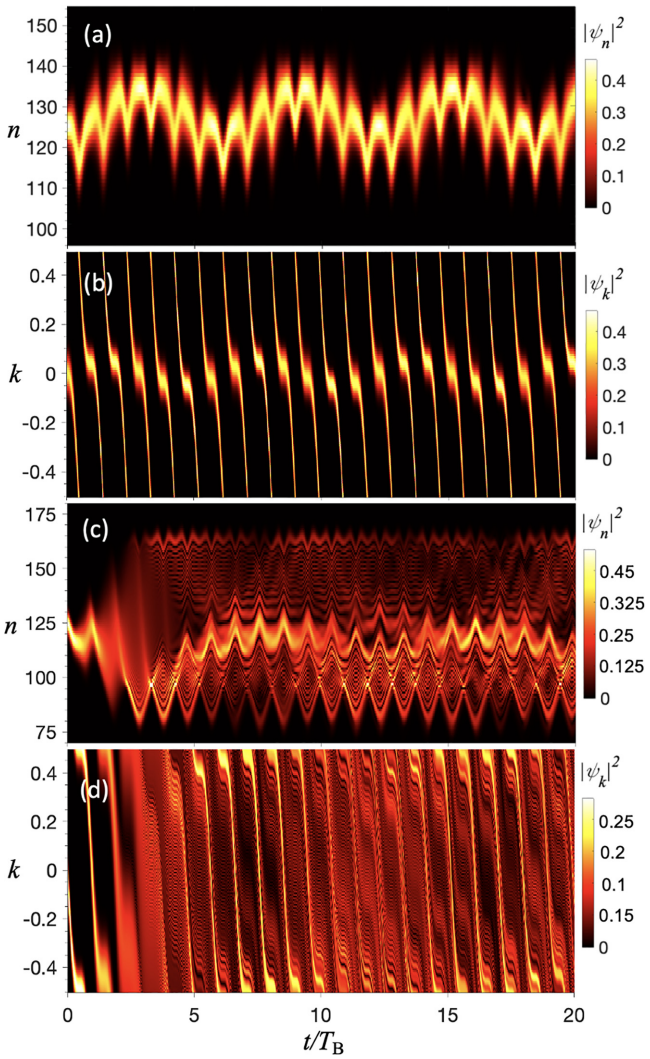

FIG. 4. Drive-phase-dependent dynamics. Time evolution of the absolute square of the real space wave function for a drive phase of (a) $\phi = -\pi/2$ and (c) $\phi = \pi/2$ exhibiting coherent CBHOs and asymmetric spreading dynamics, respectively. The corresponding quasimomentum evolutions are shown in (b) and (d), respectively.

The CBHOs shown above are accompanied by slow dephasing, which is initiated by a broadening of the wave packet at times when the transport changes direction, as shown in Fig. 2. Likewise, the wave packet evolution in k space also shows broadening, although the width in k space is inverse to the width in real space. In the presence of broadening, a collapse of the coherent oscillations occurs, and the long time dynamics are heavily dephased. To analyze the dephasing, we plot the time evolution of the width in real space, i.e., the square root of the variance, in Fig. 3. Starting with the first chirped Bloch-harmonic period, we note that the width mainly increases when the wave packet moves against the force and becomes smaller during the motion in the direction of the force. However, the initial width is never returned after the first Bloch period (see insets in Fig. 3), and there is overall growth every chirped Bloch-harmonic period. The width is reduced at the start of the second CBHO, which again increases in addition to the growth factor from the previous oscillation.

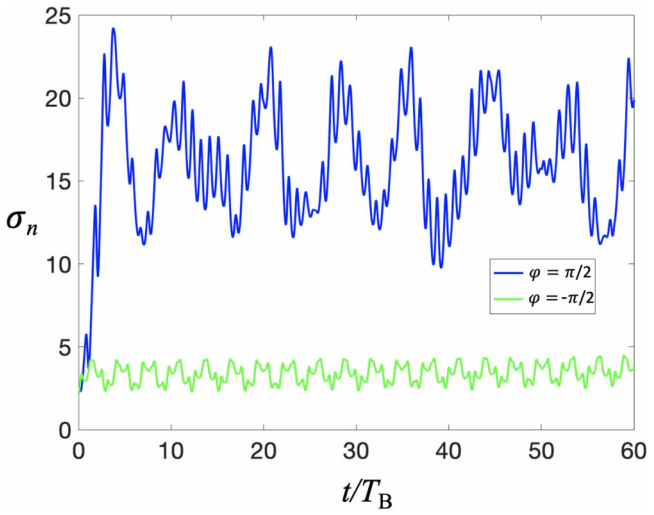

FIG. 5. Time dependence of the wave packet width in real space for drive phases of $\phi = \pi/2$ (blue) and $\phi = -\pi/2$ (green).

This pattern is repeated until the width reaches a maximum value. The oscillation of the width continues, and it saturates until an interval of coherent dynamics reappears. The inset at the right bottom of Fig. 2 shows that for long times, the wave packet gets narrower, and at a time equal to 680 T_B a revival occurs.

As shown in Fig. 4(a), a dephasing of the wave packet is not present if we drive the system with an initial phase of $\phi = -\pi/2$. In this case, coherent CBHOs emerge, which remain intact even on long time scales, however, the amplitude is reduced due to the opposite polarity of drive to BOs. The vanishing of dephasing can be attributed to a reduction in the amplitude and correspondingly decreased spatially varying effects. Figure 4(b) shows the same behavior in k space. The modulation appears immediately with a relative phase following a sine wave form, which is again confined near the center of the BZ. Thus, the interaction between BO and the modulation takes place at small values of quasimomentum, and accordingly, the real space CBHOs are smaller in amplitude.

At this point, we note that the amplitude of the CBHOs can be enhanced by modulations that modify the BO dynamics at larger absolute values of the quasi-momentum. In Fig. 4(c) we show the real space dynamics for such a case where we modulate the system with a phase of $\phi = \pi/2$. Clearly, we see an increase in the amplitude of the wave packet transport, however, we find a new kind of dynamics that corresponds to a superposition of breathing and center-of-mass Bloch dynamics. In contrast to the coherent CBHOs reported above, the wave packet distribution now spreads rapidly. The wave packet stretches in space, and we can identify two regions of unequal densities, where at one end, with a higher density toward the direction of force, the wave packet performs purely breathing dynamics, and at the other end, with a lower density, it undergoes anharmonic breathing. Both breathing oscillations occurring at a difference of $0.5T_B$ pass on the maximum density to a revival of the coherent BOs in just six Bloch periods. Furthermore, we see all three types of oscillations happening at the same time with periodic changes in density.

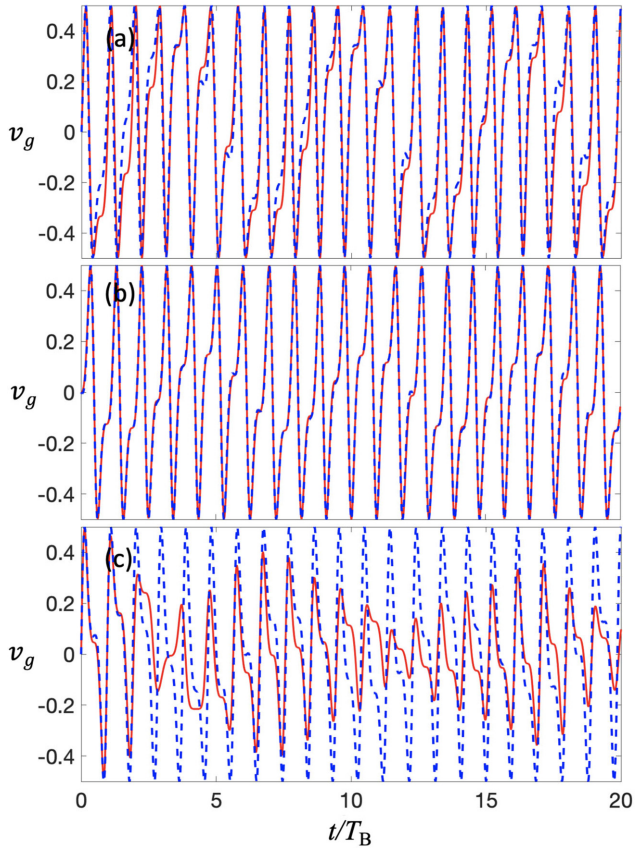

FIG. 6. Group velocity as a function of time for (a) $\phi = 0$, (b) $\phi = -\pi/2$, and (c) $\phi = \pi/2$. The red line represents the result of numerical calculations, while the dashed blue line depicts the dependence obtained from Eq. (6). For (a) the parametric values are $\Delta F = 3.65 \times 10^{-4}\ E_R$ and $\hbar\delta\omega = 5.43 \times 10^{-4}\ E_R$, while in (b) and (c) $\Delta F = 2.13 \times 10^{-4}\ E_R$. All the other parameters are the same as used previously.

The modulation appearing near the edges of the BZ is also responsible for the wave packet spreading. This is evidenced by the wave packet evolution in k space. Figure 4(d) highlights the sustained momenta near both edges, which correspond to real space motion in opposite directions and by which the wave packet spreads at times when Bragg reflections occur. One can also interpret this in terms of negligible cycle-averaged momentum. We see that the average momentum slowly increases due to the varying Bloch frequency, and thus an asymmetric spreading is generated. Then again, the wave packet gets narrower due to phase mixing and continues to follow a combination of breathing and coherent dynamics.

Note that the spreading oscillations reported here are similar in nature to the ballistic spreading regime that appears for the modulation of the periodic lattice with a constant force at the drive phases $\phi = -\pi/2, \pi/2$ [22,23,26,27]. However, under the driving with a position-dependent force at $\phi = \pi/2$ we find an asymmetrical spreading motion that dies out in a few Bloch periods and that, unlike ballistic spreading, gives rise to a mix of breathing and coherent Bloch dynamics. Also, contrastingly, we find CBHOs at a drive phase of $\phi = -\pi/2$.

In Fig. 5 we present the width variations in real space for wave packets evolving for opposite drive phases. These we compare with each other and with the width dynamics of a zero-phase drive, which we have discussed earlier. Here, the width for a $\phi = -\pi/2$ drive is seen to follow the oscillatory width profile of the $\phi = 0$ case. However, in this case the width periodically returns to its initial value and there is no overall growth. The small-width oscillations are sustained even at longer times and we perceive the case of $\phi = -\pi/2$ as a purely coherent regime of CBHOs. On the contrary, the width increases sharply for the drive phase $\phi = \pi/2$, reaching a value that is much larger than the maximum width reached in the $\phi = 0$ dynamics. The width again saturates following even larger width oscillations, but it remains far above the initial value and we do not see a complete revival in the dynamics for $\phi = \pi/2$.

We analyze the obtained complex dynamics further by comparing them to the local acceleration model. Taking into account the weak parabolic trap considered here, the local acceleration theorem with the position- and time-dependent force of our problem gives

$$\hbar\dot{k}_c(t) = -2K(t)n_c(t)/d. \tag{6}$$

With regard to BO dynamics in the absence of trap modulation, within the semiclassical approach, the spatial-variations during BOs have negligible effect on the dynamics (see the Appendix). Therefore, following the harmonic oscillator-like transport during CBHOs, we approximate that the wave packet's center in real space moves according to $n_c(t) = n_0 + \Delta n \sin(\delta\omega t + \gamma)$. Thus, on solving Eq. (6) we get $k_c(t)$, and by the perturbation method, the group velocity is given as

$$\begin{aligned} v_g(t) = \frac{Jd}{\hbar}\sin\Bigg[k_o d - \frac{F_{n_0}d}{\hbar}t + \frac{F_{n_0}d\alpha}{\hbar\omega_D}\{\cos(\omega_D t + \phi) \\ - \cos(\phi)\} + \frac{\Delta F d}{\hbar\delta\omega}\{\cos(\delta\omega t + \gamma) - \cos(\gamma)\} \\ \pm \frac{\Delta F d\alpha}{\hbar(\omega_D \pm \delta\omega)}\{\sin((\omega_D \pm \delta\omega)t + (\phi \pm \gamma)) \\ - \sin(\phi \pm \gamma)\}\Bigg], \end{aligned} \tag{7}$$

where ΔF is the change in force across spatial distance Δn, and $\delta\omega$ is the frequency of CBHOs. Equation (7) is plotted in Fig. 6 where the analytical result is compared with the numerically calculated dynamics of the group velocity. The parameters Δn and $\delta\omega$ are particular to the system, and we extract these from the real space dynamics shown above. Figure 6(a) shows that for $\phi = 0$ the semiclassical and approximate analytical result covers the relative phase of CBHOs quite well. However, in this case, the spatially varying effects are quite significant and cannot be fully captured by the approximate model, so no exact match between numerics and Eq. (7) is obtained. For the case of $\phi = -\pi/2$ shown in Fig. 6(b) we achieve a very good agreement between Eq. (7) and the numerical calculations, and the rapid oscillations of the relative phase are also confirmed. Clearly, the insertion of an oscillatory function put restrictions on the relative phase such that the modulation now does not affect the entire velocity values unless $\delta\omega$ is very small. Figure 6(c) shows the breakdown of our analytical model, which is due to the spreading and the multimode dynamics present for $\phi = \pi/2$ which are beyond the semiclassical model.

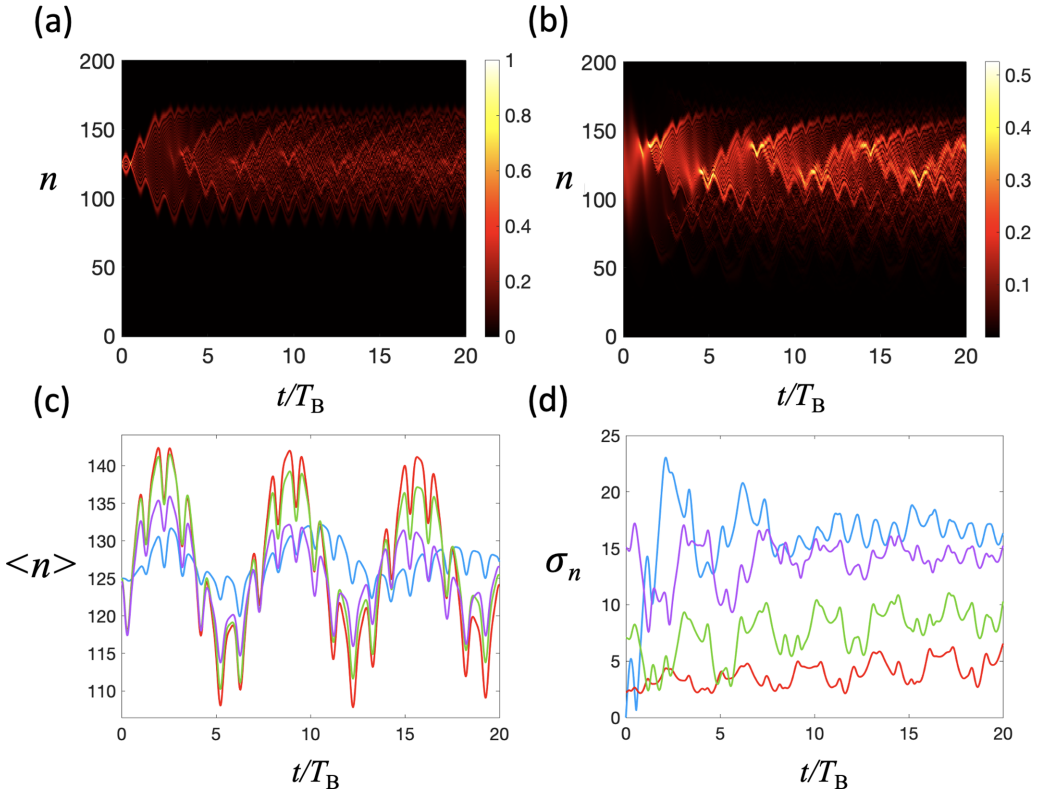

FIG. 7. CBHOs for different choices of initial widths of $\sigma = 0.025$ (a) and $\sigma = 15.811$ (b). Dynamics of the average position (c) and width variance (d) for $\sigma = 0.025$, 2.236, 7.071, and 15.811 represented by the blue, red, green, and purple lines, respectively. The results correspond to the case of $\phi = 0$ phase drive.

Next, we discuss the effect of different initial widths on the CBHOs. Figure 7 shows a comparison of the dynamics when choosing various initial widths for our Gaussian wave packet. It is seen that the overall character of the dynamics remains similar for significantly wider or sharply narrower widths. As expected, a sharply localized wave packet performs breathing dynamics, as shown in Fig. 7(a). However, unlike breathing SBOs, the spreading wave packet partially contracts, and the overall evolution is similar to the dynamics of a sharply localized harmonic oscillator wave packet placed on a periodic lattice. The wave packet contracts every half chirped Bloch-harmonic period due to phase matching, which is then followed by expansion again. This continuous and the overall dynamics dephase in just a few chirped Bloch-harmonic periods. Likewise, a wide wave packet, in Fig. 7(b), is also seen to exhibit spreading chirped Bloch-harmonic motion where the dispersion takes place due to wave packet narrowing induced by a self-phase mixing emerging from the spatially varying force. Alongside, some weak fraction of the wave packet is initially seen to undergo large transport, which then interferes with the spreading wave packet and gives rise to more complex dynamics. Figures 7(c) and 7(d) further illustrate a qualitative resemblance in the dynamics with the width choices discussed above, which are compared against two other instances of chosen intermediate widths. The results for a sharply localized width (blue curves) highlight the modulated oscillations of the mean position, and variance sustained around a high value which confirm the harmonic oscillatorlike spreading and the differences from breathing SBOs. Also, for a much wider wave packet (purple curves), the mean position oscillates with a decaying amplitude, which is due to the spreading dynamics and the related dephasing. The variance in this case first decreases, reaching a minimum corresponding to the wave packet narrowing, and then increases, leading to further width oscillations. In these cases, the complex-width oscillations are attributed to the expansion and partial contraction of the wave packet during evolution. In the intermediate width cases, the results show large-amplitude CBHOs of the mean position and a slow-gradual increase in the width. We note that the slow increase in width is due to weakly dephased dynamics at $\phi = 0$ drive phase, and thus the CBHOs are maximally coherent for a moderately wide wave packet. Hence, the dynamics are highly sensitive to the initial width of the wave packet and the choice of a localized wave packet with moderate width is crucial for the application of the presented semiclassical model. This knowledge is important for characterizing the system's response and designing experiments or control strategies tailored to specific requirements or desired outcomes. Further, we describe the dynamics with a different initial position for our wave packet. Note that for a fixed driving frequency, a shift in initial position is equivalent to driving the system with frequencies beyond the primary resonance, as a change in position n_0 redefines the initial Bloch frequency. In Fig. 8(a) we show the dynamics for the Gaussian wave packet placed at site $n_0 = 150$, under the same driving frequency as used before, i.e., $\hbar\omega_D = 0.0038\ E_R$, which corresponds to Bloch frequency at $n = 125$. It is seen that the wave packet in this case performs CBHOs

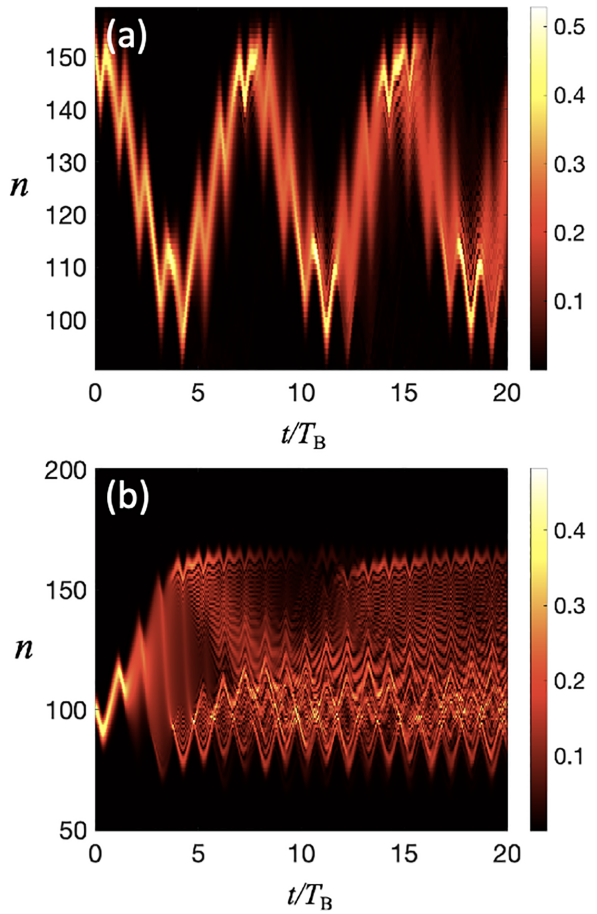

FIG. 8. CBHOs (a) and spreading dynamics (b) for the same parameters as in Fig. 2 but for the initial wave packet placed at $n_0 = 150$ and $n_0 = 100$, respectively.

around the lattice position $n = 125$. This is due to a steady modulation of the relative phase, even at small deviations from the resonance condition. We found that the phase is regular for $n_0 - n_c/2 \lesssim n_0 \lesssim n_0 + n_c/2$, which marks the regime of CBHOs where the wave packet undergoes harmonic transport around the position related to a primary resonance. Beyond this regime, the dynamics change character between spreading and complex dynamics unless a secondary resonance is triggered. In Fig. 8(b) we show spreading dynamics for a wave packet initially placed at $n_0 = 100$. The location corresponds to the boundary of the regime of CBHOs, where the relative phase is seen to oscillate near the edges of the Brillouin zone, similar to Fig. 4(d), and thus spreading dynamics are obtained.

To show dynamics arising on a secondary resonance, instead of changing the initial position n_0, we simply vary the frequency of the drive. When choosing $\omega_B = \omega_D/q$ with $q \in \mathbb{N}$, we obtain superharmonic modes, and at $\omega_B = r\omega_D$ with $r \in \mathbb{N}$ subharmonic response is seen in the dynamics. Figure 9 shows an instructive example of such scenarios. The superharmonic modes are illustrated in Figs. 9(a) and 9(b), where modulation appears rather quickly. The quick change of the relative phase is visible in the k-space evolution, which carries two distinguishable oscillatory phases on top of Bloch oscillations. The resulting dynamics manifest a fast modulation of the Bloch oscillations, which can be averaged out if the driving frequency is too high. In our numerical simulations, we have found that the dephased Bloch dynamics of the static system remain unaffected by the drive for $\omega_B \geqslant \omega_D/10$. In Figs. 9(c) and 9(d) subharmonic motion is shown, where the modulation interacts with Bloch oscillations at alternate periods. Therefore, for one Bloch period, the wave packet performs ordinary Bloch oscillations, and in the next period, the transport is generated. The resulting motion is similar to CBHOs, although the dynamics here decay rather quickly and strongly dephased dynamics are obtained. The subharmonic response demonstrated by the model makes it appropriate for an exploration of time crystals in cold atomic systems as a future endeavor.

IV. CONCLUSIONS

In summary, our calculations demonstrate that a position- and time-dependent force realized in ultracold atomic systems brings about an abundance of dynamics that are not accessible in traditional solid-state systems. The dynamics range from CBHOs, over collapse and revivals to asymmetric spreading oscillations. These are the outcomes of phase modulations induced by the spatial variations. The k-space evolution of the wave packet and the predictions of an approximate semiclassical model confirm our interpretations. Our studies provide a general protocol to analyze and predict the dynamics in more realistic material systems, where the lattice profile can be globally or locally inhomogeneous. Also, different frequency chirps can be induced in the driving field to artificially manipulate the transport or tailor the dynamics with unique oscillation profiles. These findings provide exciting opportunities for experimental verification with ultracold-atom experiments and may lead to new insights into the properties of quantum systems in confined geometries with potential applications in atomic diffraction, entanglement generation, atom interferometry, and force metrology.

ACKNOWLEDGMENT

U.A. gratefully acknowledges support from the Deutscher Akademischer Austauschdienst (DAAD) through a doctoral research grant.

APPENDIX: DYNAMICS FOR A STATIC TRAP

Here, we present our analytical approach applied to the case of the stationary system that uses a static parabolic trap, for which the solution to the acceleration relation follows,

$$k_c(t) = k_c(0) - \frac{m\omega_\tau^2}{\hbar}\int_0^t x_c(t')\,dt'. \tag{A1}$$

Considering the Bloch oscillating evolution of our wave packet, i.e. $x_c(t) = x(0) + \Delta x\cos(\omega_B t + k_c(0)d)$ with Δx and ω_B being the amplitude and initial frequency of Bloch oscillations, respectively, the above equation simplifies as

$$k_c(t) = k_c(0) - \frac{m\omega_\tau^2 x(0)}{\hbar}t - \frac{\Delta x}{dx(0)}[\sin\{\omega_B t + k_c(0)d\} - \sin\{k_c(0)d\}], \tag{A2}$$

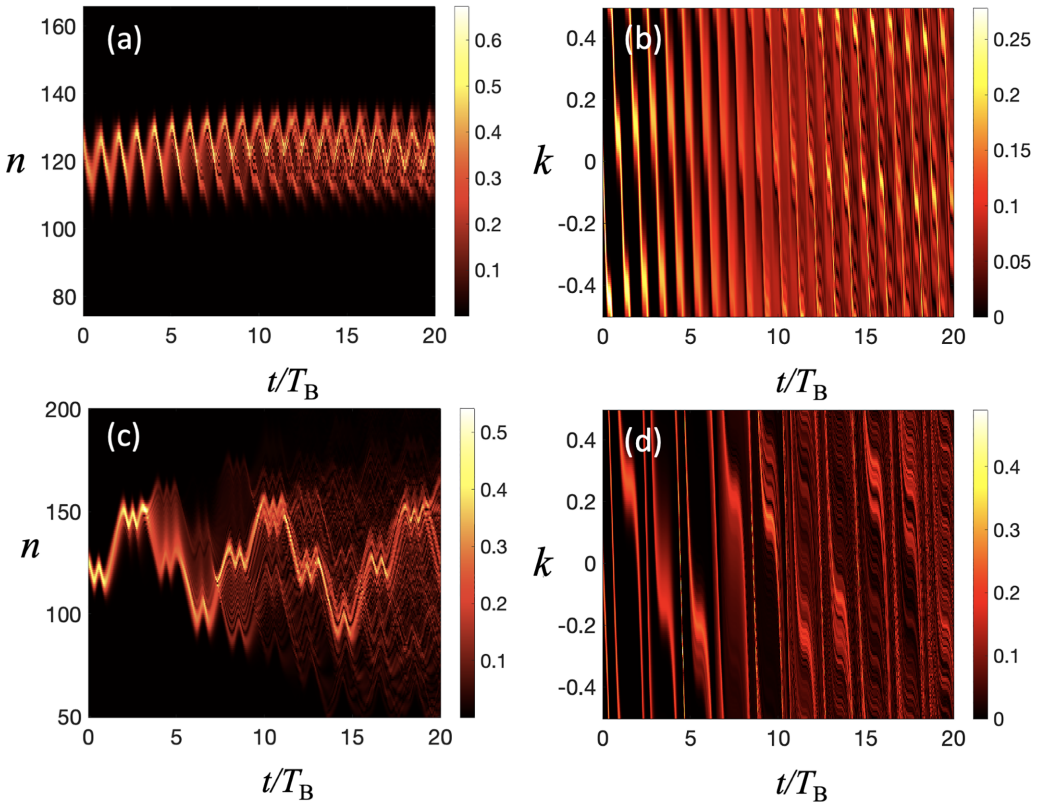

FIG. 9. Weakly modulated Bloch oscillation (a), (b) at $\omega_B = \omega_D/2$ and dynamics similar to CBHOs (c), (d) at $\omega_B = 2\omega_D$. Other parametric values remain the same as in Fig. 2.

which shows that the spatial variations during Bloch oscillations have a negligible effect on the dynamics of $k_c(t)$, as $x(0) \gg \Delta x$. The wave packet evolves with an almost constant Bloch frequency, $\omega_B \approx m\omega_\tau^2 d\, x(0)/\hbar$, where the oscillation amplitude is given by $\Delta x = J/m\omega_\tau^2 d\, x(0)$, with J being the tunneling matrix element between contiguous lattice sites [29,30].

Further, it is known that for the considered system, a regime of dipole oscillations exists for wave packets placed near the center of the parabolic potential [29,30,44]. In such situations, the real space evolution of the wave packet's center is approximated as $x_c(t) = x(0)\cos(\omega_{HO}t + k_c(0)d)$, where $\omega_{HO} = \sqrt{Jm\omega_\tau^2 d^2}/\hbar$ is the frequency of the dipolar motion across the center of the trap potential. Thus, the time evolution of the quasimomentum follows from Eq. (A1) as

$$k_c(t) = k_c(0) - \frac{m\omega_\tau^2 x(0)}{\hbar\omega_{HO}}[\sin\{\omega_{HO}t + k_c(0)d\} - \sin\{k_c(0)d\}], \tag{A3}$$

showing that the quasimomentum oscillates around the maximum value determined by $x(0)$.

[1] F. Schäfer, T. Fukuhara, S. Sugawa, Y. Takasu, and Y. Takahashi, Tools for quantum simulation with ultracold atoms in optical lattices, Nat. Rev. Phys. **2**, 411 (2020).

[2] A. J. Allen, N. G. Parker, N. P. Proukakis, and C. F. Barenghi, Quantum turbulence in atomic Bose-Einstein condensates, J. Phys.: Conf. Ser. **544**, 012023 (2014).

[3] L. Tarruell and L. Sanchez-Palencia, Quantum simulation of the Hubbard model with ultracold fermions in optical lattices, C. R. Phys. **19**, 365 (2018).

[4] M. Łącki, H. Pichler, A. Sterdyniak, A. Lyras, V. E. Lembessis, O. Al-Dossary, J. C. Budich, and P. Zoller, Quantum Hall physics with cold atoms in cylindrical optical lattices, Phys. Rev. A **93**, 013604 (2016).

[5] M. Schreiber, S. S. Hodgman, P. Bordia, H. P. Lüschen, M. H. Fischer, R. Vosk, E. Altman, U. Schneider, and I. Bloch, Observation of many-body localization of interacting fermions in a quasirandom optical lattice, Science **349**, 842 (2015).

[6] P. M. Preiss, R. Ma, M. Eric Tai, A. Lukin, M. Rispoli, P. Zupancic, Y. Lahini, R. Islam, and M. Greiner, Strongly correlated quantum walks in optical lattices, Science **347**, 1229 (2015).

[7] F. Meinert, M. Knap, E. Kirilov, K. Jag-Lauber, M. B. Zvonarev, E. Demler, and H.-C. Nägerl, Bloch oscillations in the absence of a lattice, Science **356**, 945 (2017).

[8] Z. A. Geiger, C. Fujiwara, K. Singh, R. Senaratne, S. V. Rajagopal, M. Lipatov, T. Shimasaki, R. Driben, V. V. Konotop, T. Meier, and D. M. Weld, Observation and uses of position-space Bloch oscillations in an ultracold gas, Phys. Rev. Lett. **120**, 213201 (2018).

[9] F. Bloch, Über die Quantenmechanik der Elektronen in Kristallgittern, Z. Phys. **52**, 555 (1929).

[10] S. Arlinghaus and M. Holthaus, Generalized acceleration theorem for spatiotemporal Bloch waves, Phys. Rev. B **84**, 054301 (2011).

[11] V. Grecchi and A. Sacchetti, Acceleration theorem for Bloch oscillators, Phys. Rev. B **63**, 212303 (2001).

[12] H. Jones and C. Zener, The general proof of certain fundamental equations in the theory of metallic conduction, Proc. R. Soc. London A **144**, 101 (1934).

[13] C. Zener, A theory of the electrical breakdown of solid dielectrics, Proc. R. Soc. London A **145**, 523 (1934).

[14] U. Peschel, T. Pertsch, and F. Lederer, Optical Bloch oscillations in waveguide arrays, Opt. Lett. **23**, 1701 (1998).

[15] R. Morandotti, U. Peschel, J. S. Aitchison, H. S. Eisenberg, and Y. Silberberg, Experimental observation of linear and nonlinear optical Bloch oscillations, Phys. Rev. Lett. **83**, 4756 (1999).

[16] M. Ben Dahan, E. Peik, J. Reichel, Y. Castin, and C. Salomon, Bloch oscillations of atoms in an optical potential, Phys. Rev. Lett. **76**, 4508 (1996).

[17] S. R. Wilkinson, C. F. Bharucha, K. W. Madison, Q. Niu, and M. G. Raizen, Observation of atomic Wannier-stark ladders in an accelerating optical potential, Phys. Rev. Lett. **76**, 4512 (1996).

[18] J. Feldmann, K. Leo, J. Shah, D. A. B. Miller, J. E. Cunningham, T. Meier, G. von Plessen, A. Schulze, P. Thomas, and S. Schmitt-Rink, Optical investigation of Bloch oscillations in a semiconductor superlattice, Phys. Rev. B **46**, 7252 (1992).

[19] A. M. Bouchard and M. Luban, Bloch oscillations and other dynamical phenomena of electrons in semiconductor superlattices, Phys. Rev. B **52**, 5105 (1995).

[20] T. Hartmann, F. Keck, H. J. Korsch, and S. Mossmann, Dynamics of Bloch oscillations, New J. Phys. **6**, 2 (2004).

[21] M. Holthaus, Bloch oscillations and Zener breakdown in an optical lattice, J. Opt. B: Quantum Semiclass. Opt. **2**, 589 (2000).

[22] K. Kudo and T. S. Monteiro, Theoretical analysis of super-Bloch oscillations, Phys. Rev. A **83**, 053627 (2011).

[23] A. R. Kolovsky and H. J. Korsch, Dynamics of interacting atoms in driven tilted optical lattices, J. Siberian Federal Univ.: Math. Phys. **3**, 311 (2010).

[24] Q. Thommen, J. C. Garreau, and V. Zehnlé, Theoretical analysis of quantum dynamics in one-dimensional lattices: Wannier-Stark description, Phys. Rev. A **65**, 053406 (2002).

[25] J. Wan, C. Martijn de Sterke, and M. M. Dignam, Dynamic localization and quasi-Bloch oscillations in general periodic ac-dc electric fields, Phys. Rev. B **70**, 125311 (2004).

[26] A. Alberti, V. V. Ivanov, G. M. Tino, and G. Ferrari, Engineering the quantum transport of atomic wavefunctions over macroscopic distances, Nat. Phys. **5**, 547 (2009).

[27] E. Haller, R. Hart, M. J. Mark, J. G. Danzl, L. Reichsöllner, and H.-C. Nägerl, Inducing transport in a dissipation-free lattice with super Bloch oscillations, Phys. Rev. Lett. **104**, 200403 (2010).

[28] E. Díaz, A. G. Mena, K. Asakura, and C. Gaul, Super-Bloch oscillations with modulated interaction, Phys. Rev. A **87**, 015601 (2013).

[29] A. V. Ponomarev and A. R. Kolovsky, Dipole and Bloch oscillations of cold atoms in a parabolic lattice, Laser Phys. **16**, 367 (2006).

[30] J. Brand and A. R. Kolovsky, Emergence of superfluid transport in a dynamical system of ultra-cold atoms, Eur. Phys. J. D **41**, 331 (2007).

[31] K. W. Mahmud, L. Jiang, E. Tiesinga, and P. R. Johnson, Bloch oscillations and quench dynamics of interacting bosons in an optical lattice, Phys. Rev. A **89**, 023606 (2014).

[32] J.-P. Gallinar and E. Chalbaud, Harmonic oscillator on a lattice in a constant force field and associated Bloch oscillations, Phys. Rev. B **43**, 2322 (1991).

[33] S. Longhi, Bloch dynamics of light waves in helical optical waveguide arrays, Phys. Rev. B **76**, 195119 (2007).

[34] M. J. Zheng, Y. S. Chan, and K. W. Yu, Steering between Bloch oscillation and dipole oscillation in parabolic optical waveguide arrays, J. Opt. Soc. Am. B **27**, 1299 (2010).

[35] M. J. Zheng, Y. S. Chan, and K. W. Yu, Harmonic oscillations and their switching in elliptical optical waveguide arrays, J. Opt. **13**, 035708 (2011).

[36] M. J. Zheng, Y. S. Chan, and K. W. Yu, Photonic Bloch-dipole-Zener oscillations in binary parabolic optical waveguide arrays, J. Opt. Soc. Am. B **28**, 1339 (2011).

[37] N. Mann, M. Reza Bakhtiari, F. Massel, A. Pelster, and M. Thorwart, Driven Bose-Hubbard model with a parametrically modulated harmonic trap, Phys. Rev. A **95**, 043604 (2017).

[38] J. Bera, A. Q. Batin, S. Ghosh, B. Malomed, and U. Roy, Generation of higher harmonics in dipolar Bose-Einstein condensates trapped in periodically modulated potentials, Philos. Trans. R. Soc. A **381**, 20220075 (2023).

[39] A. Cao, R. Sajjad, E. Q. Simmons, C. J. Fujiwara, T. Shimasaki, and D. M. Weld, Transport controlled by Poincaré orbit topology in a driven inhomogeneous lattice gas, Phys. Rev. Res. **2**, 032032(R) (2020).

[40] R. Grimm, M. Weidemüller, and Y. B. Ovchinnikov, Optical dipole traps for neutral atoms, Adv. At. Mol. Opt. Phys. **42**, 95 (2000).

[41] M. M. Neiczer, Efficient creation of a molecular Bose-Einstein condensate of Lithium-6 using a spatially modulated dipole trap, Master Thesis, University of Heidelberg, 2018.

[42] W. Zwerger, Mott-Hubbard transition of cold atoms in optical lattices, J. Opt. B: Quantum Semiclass. Opt. **5**, S9 (2003).

[43] M. Ayub, K. Naseer, M. Ali, and F. Saif, Atom optics quantum pendulum, J. Russ. Laser Res. **30**, 205 (2009).

[44] A. M. Rey, G. Pupillo, C. W. Clark, and C. J. Williams, Ultracold atoms confined in an optical lattice plus parabolic potential: A closed-form approach, Phys. Rev. A **72**, 033616 (2005).

[45] D. McKay, M. White, and B. DeMarco, Lattice thermodynamics for ultracold atoms, Phys. Rev. A **79**, 063605 (2009).

[46] F. S. Cataliotti, L. Fallani, F. Ferlaino, C. Fort, P. Maddaloni, and M. Inguscio, Superfluid current disruption in a chain of weakly coupled Bose-Einstein condensates, New J. Phys. **5**, 71 (2003).